Article

Cell Adhesion Assessment Reveals a Higher Force per Contact Area on Fibrous Structures Compared to Flat Substrates

Ana Sancho, Mehmet Berat Taskin, Laura Wistlich, Philipp Stahlhut, Katharina Wittmann, Angela Rossi, and Jürgen Groll*
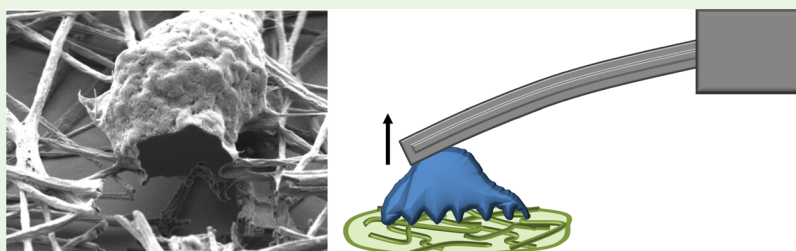
Cite This: https://doi.org/10.1021/acsbiomaterials.1c01290

Read Online

ACCESS | 📊 Metrics & More | 📰 Article Recommendations | 🆘 Supporting Information

ABSTRACT: The distribution and density of ligands have a determinant role in cell adhesion on planar substrates. At the same time, planar surfaces are nonphysiological for most cells, and cell behavior on planar and topographical surfaces is significantly different, with fibrous structures being the most natural environment for cells. Despite phenomenological examinations, the role of adhesion ligand density in the fibrous scaffold for cell adhesion strength has so far not been assessed. Here, we established a method to measure the amount of cell ligands on biofunctionalized electrospun meshes and planar substrate coatings with the same chemical composition. With this as a basis for systematic comparison and pure polyester as benchmark substrates, we have cultured L929 mouse fibroblasts and measured the adhesion force to surfaces of different chemistry and topography. In every case, having fibrous structures have led to an increased adhesion force per area also at a lower ligand density, which remarks the importance of such structures in a natural extracellular environment. Conversely, cells migrate more on planar surfaces than on the tested fibrous substrates. We thus established a platform to study cell–matrix interactions on different surfaces in a precise and reproducible manner as a new tool to assess and quantify cell–matrix interactions toward 3D scaffolds.

KEYWORDS: cell adhesion, single-cell force spectroscopy, single-cell force microscopy, biomimicry, 3D structures, cell–material interaction

1. INTRODUCTION

Understanding how cells interact with the surrounding environment is an important milestone in the study of biological processes and a prerequisite for the development of bespoke biomaterials and scaffolds. Cell–material interactions have so far widely been investigated in 2D geometries, e. g., by growing cells on planar surfaces such as plastic or glass that were coated with cell adhesion ligands either in homogeneous planar distribution or in patterns. These efforts primarily focused on understanding cell adhesion mechanisms and the influence of ligand density by analyzing distributions of relevant biomolecules and downstream cellular pathways.[1−4] Also, the effects of more complex substrate designs such as locally manipulated ligand densities[5,6] and nanotopographical patterns with tailor-made sizes, shapes, and spacings on cell–substrate interactions were investigated.[7] Studying cell–material interactions on flat and easy-to-analyze 2D model substrates thus leads to a wealth of knowledge, for example, about the threshold ligand density per surface area and even the inter-ligand distance needed to facilitate proper cell adhesion.

Such fundamental studies were later combined with analysis of cell adhesion forces, initially using single-cell force spectroscopy.[8,9] Quantifying the adhesion force of cells to the underlying material by cell detachment becomes challenging as the focal adhesions get mature since the immobilization of the cell to the measuring probe needs to be strong enough to overcome the adhesion forces exerted onto the substrate.[10,11] Therefore, usually, either the experimental time points are limited to a few minutes of contact time between the cell and the substrate or the measuring probes are chemically functionalized to increase the force range.[12] The novel FluidFM technology overcomes this limitation by allowing high immobilization forces through the integration of a microfluidic channel into the cantilevers, which allows the

A

application of under-pressure at the cell membrane.[13−16] FluidFM was used as a tool in quantifying adhesion forces of endothelial cells to substrates with different depths of grooves.[17] More recently, FluidFM was also used to analyze intercellular adhesion forces in confluent cell monolayers[15] and to assess the effect of coating 2D substrates with ECM proteins such as fibronectin and collagen I on early and mature adhesion forces of L929 fibroblast and MC3T3 osteoblasts.[18]

While 2D model substrates are easy for standardization and analysis, this simplicity comes at the expense of poor mimicry of the psychological 3D cell environment, the extracellular matrix (ECM). The ECM is a complex biological micro-environment, largely composed of fibrillar proteins that are embedded in a hydrogel matrix. Apart from providing structural stability to tissues, the fibrous protein network also offers various anchor points for cells to adhere to through a series of transmembrane proteins called integrins.[19] Cells grow in this organized 3D environment, but it is a combination of cell−cell and cell−matrix interactions that orchestrate cellular processes such as proliferation, differentiation, apoptosis, or invasion. Accordingly, cells behave differently on materials that mimic the 3D ECM complexity than on unphysiological 2D substrates, for example, by having significantly different levels of focal or fibrillar adhesions. A similar difference is also observed in the presence as well as the distribution of contributing proteins such as paxillin.[20] These considerations indicate that basic cellular processes, i.e., cell adhesion force, and also the threshold of ligand density and the overall amount needed for cell adhesion, are different in 3D substrates and should rather be studied using 3D matrices to more closely understand in vivo cell biology.[21,22]

Previously, we reported the functional prepolymer sP(EO-*stat*-PO) that dramatically alters the properties of biomaterial surfaces by providing a dense nonfouling layer that inhibits cell adhesion. Furthermore, using the robust isocyanate chemistry, this nonfouling coating was functionalized with cell adhesion motifs effectively controlling the cell attachment process.[23,24] As electrospinning is an efficient technique to produce scaffolds that resemble the 3D fibrous structural component of the ECM,[25] we also previously combined this approach with electrospinning where sP(EO-*stat*-PO), conjugated with cell adhesion peptides, was blended with hydrolytically degradable polyester, PLGA. The obtained fibrous scaffold yielded a remarkable nonfouling interface that greatly deterred non-specific protein adsorption while facilitating strong cell−substrate interactions such as attachment, spreading, and migration.[26−28] However, surface-sensitive quantification of biofunctionalization on electrospun fibrous scaffolds is challenging[29] and hence there is still little known about how the density of biomolecules drives the cell attachment process in the ECM mimicking 3D fibrillar environment.

In this study, we analyzed cell adhesion forces on fibrous substrates even under low fiber density conditions using FluidFM. Following the previously established methods, we fabricated fibrous scaffolds from a biodegradable and biocompatible copolymer, PLGA, by electrospinning polymer solution on glass coverslips. To facilitate cell−fiber interaction, we immobilized the cell adhesion-mediating peptide RGD on PLGA fibers by co-spinning PLGA solution blended with a reactive hydrophilic prepolymer, NCO-sP(EO-*stat*-PO), where peptides covalently bind via robust isocyanate chemistry. As it is vital to isolate the effect of the underlying glass surface on cell adhesion, coverslips were made nonfouling for cells but

made to fix electrospun fibers on the surface via NCO-sP(EO-*stat*-PO) coating. This allowed cells only to adhere to fibers and fibers to firmly remain in position during the process of cell detachment via a FluidFM probe. We further applied a novel UV-spectroscopy-based method to quantitatively determine the amount of immobilized peptides on both flat and fibrous substrates. We then assessed cell spreading and expression of a focal adhesion molecule, vinculin, and finally tracked cellular migration patterns of the cells. The obtained results were analyzed and discussed in comparison to 2D polymer substrates to identify the effect of topographical factors on cell adhesion and migration. Our results show minor differences in adhesion forces on substrates of different chemical compositions and an increase in the adhesion force exerted per area on fibrous scaffolds in comparison to flat substrates. We have also tracked the migration patterns on both and noticed a more extensive migration on the planar case.

2. MATERIALS AND METHODS

2.1. Electrospinning of Functionalized and Nonfunctional-ized Fibers. The spinning solution of the PLGA fibers was prepared as described before[27] by dissolving PLGA (Resomer RG 504, Evonik, Germany) at 24.5 wt % in a mixture of dry dimethyl sulfoxide (DMSO) and acetone (ratio of 1:5 V/V) and stirred until fully dissolved. For samples containing NCO-sP(EO-*stat*-PO), the prepolymer was first dissolved in (DMSO) and stirred for 10 min. The solution was then diluted with acetone and briefly mixed, and finally, PLGA was added and stirred until the solution was homogeneous. The polymer content of the solution was 5 wt % for NCO-sP(EO-*stat*-PO) and 24.5 wt % for PLGA. Polymer solutions were fed at 0.5 mL/h through a flat-tip stainless steel spinneret connected to a high-voltage power supply, and a high voltage of 13 kV was applied to the spinning solution. The collection distance between the spinneret and grounded collector was 15 cm. The nonwoven meshes were collected on a rotating drum as a grounded collector (diameter of 60 mm, length of 100 mm) with a rotation speed of 140 rpm. The molecular weight of sP(EO-*stat*-PO) was 12 kDa, and for PLGA, the Mw was 75 kDa. Electrospinning typically resulted in a random distribution of nonwoven PLGA fibers with a mean diameter of 562 ± 86 nm (mean ± SD) and nonwoven PLGA-sP(EO-*stat*-PO)-RGD fibers with a mean diameter of 568 ± 149 nm. During electrospinning, the NCO-sP(EO-*stat*-PO) content was previously shown to be surface-segregated, leading to enrichment of NCO-sP(EO-*stat*-PO) on fiber surfaces that contribute to the hydrophilicity of the scaffolds and may facilitate enhanced presentation of conjugated bioactive molecules.

2.2. Quantitative Determination of Peptide Concentrations. Different amounts of the model peptide were dissolved in tris(2-carboxyethyl) phosphine (TCEP) (3.4×10^{-5} mol/mL) in 0.1 N NaOH and assessed by UV-spectroscopy to obtain the calibration curve (Figure S1). The pH was kept neutral (pH = 7.4) and controlled regularly since the UV-absorption of mercaptopyridine is pH-dependent. From the solution, a serial dilution was prepared, and the absorbance was measured at 270 nm. To determine the peptide concentration on the surface of the fibers, fiber meshes were produced by adding the model peptide to the NCO-sP(EO-*stat*-PO)/PLGA solution and electrospinning them directly on the collector. Afterward, the mesh was incubated for 96 h under ambient conditions to remove the residual solvents, which could bias the results, and to allow cross-linking. To quantify peptide concentrations and peptide binding mode, membranes were cut into pieces of 4 × 6 cm and weighted. Afterward, the membranes were placed in bacterial dishes and incubated in deionized water (2 mL) for 24 h. It followed a 24 h incubation in 2 mL of TCEP solution (3.4×10^{-5} mol/mL in 0.1 N NaOH) and then 24 h in 1 N NaOH (1.15 mL). TCEP solution (6.8×10^{-5} mol/mL in 0.2 N NaOH) was added to the washing water and 3.4×10^{-4} mol/mL TCEP to the NaOH suspension. Subsequently, all

solutions were measured UV-metrically at 270 nm. With the calibration curve, the peptide concentration was calculated by measuring the absorbance of the membrane.

2.3. Preparation of Planar Substrates for Cell Culture. Glass slides (diameter of 15 mm, Marienfeld, Lauda-Königshofen, Germany) were cleaned with isopropanol and then ultrasonicated with acetone, H_2O, and isopropanol for 10 min at 40 °C. The slides were activated with plasma, and subsequently, aminosilylation was performed in an exicator by use of (3-aminopropyl)trimethoxysilane (Sigma Aldrich, Germany). The coating of glass substrates was done as described before.[30] Briefly, prepolymers NCO-sP(EO-*stat*-PO) were dissolved in dry THF and H_2O was added in a ratio of 1:9 (THF/H_2O) to achieve a prepolymer concentration of 10 mg/mL. For experiments with peptide addition, the desired amount of H-CGRGDS-OH (GeneCust, Ellange, Luxembourg) to achieve a molar ratio of 2:1, 5:1, or 10:1 (peptide:prepolymer) was mixed with water and added to NCO-sP(EO-*stat*-PO) dissolved in THF.[23] For spin-coating, the substrates were placed on the device under vacuum, covered with the solution, and subsequently accelerated to 2500 rpm with an acceleration time of 5 s. The device operated for 40 s. The resulting NCO-sP(EO-*stat*-PO) coatings were stored overnight at room temperature to complete the cross-linking.

For PLGA flat surfaces, films were processed with a film cast device (Coatmaster 510, Erichsen, Hemer, Germany). Therefore, a 25% solution of PLGA in dichloromethane (DCM, Sigma Aldrich, Germany) was prepared and cast with a speed of 5 mm/s and a thickness of 120 μm. After drying for several days, the film was used for cell tests by transferring it into cell crowns (Minucells and Minutissue GmbH, Bad Abbach, Germany), sterilizing it with 70% ethanol and washing it with phosphate buffered saline (PBS) three times.

2.4. Preparation of Fibrous Substrates for Cell Culture. Cover glasses were cleaned and coated with NCO-sP(EO-*stat*-PO) solution as explained above and transferred to the collector of the electrospinning device. The polymer solutions were electrospun on the coated cover glasses under the same conditions and parameters described above. After electrospinning times of 4 and 8 min for pure PLGA fibers and 30 s and 3 min for NCO-sP(EO-*stat*-PO)/PLGA fibers, the process was stopped and the glass slides were removed carefully from the drum and sterilized with a UV lamp.

2.5. Measurement of Cell Adhesion Forces by FluidFM. Adhesion forces of L929 mouse fibroblasts to the underlying fibers were measured by single-cell force spectroscopy (SCFS). More precisely, FluidFM technology (Cytosurge AG, Switzerland) was adapted to an atomic force microscope (AFM) of model Flex-FPM (Nanosurf GmbH, Germany), which was mounted on top of an inverted Axio Observer Z1 microscope (Carl Zeiss, Germany). The measurement of the adhesion forces was performed by complete detachment of the cells, as explained before.[15] Briefly, when the 8 μm-aperture micropipette cantilever of 2 N/m nominal spring constant (Cytosurge AG, Switzerland) reaches the surface of the cell, an underpressure is applied through the fluidic system. This underpressure immobilizes the cell at the tip of the cantilever, allowing complete detachment of the cell from the underlying material with the cantilever retraction. Deflection of the cantilever during retraction is recorded, which is proportional to the adhesion force. The maximum cantilever deflection corresponds to the so-called maximum detachment force (MDF), which has been considered as the representative adhesion force throughout this work.

2.6. Calculation of Cell Spreading and Contact Areas. Bright-field images were taken with an Axio Observer Z1 microscope using a 40× objective. For the calculation of the cell spreading area, the perimeter of the cells was outlined and the surrounded area was automatically calculated by use of ImageJ open software (NIH, https://imagej.nih.gov/ij/). In planar surfaces, the contact area between the cells and the substrates is equal to the cell spreading area. By contrast, in the fibrous substrates, the cell–substrate contact area corresponds to the segment of fibers, excluding the underlying material, that are located under the cell and in direct contact with it. This region was outlined in ImageJ and likewise calculated.

2.7. Slicing and Visualization of Cells by Electron Microscopy. In order to verify that L929 mouse fibroblasts adhere only onto the fibers and not underneath them, cross-sectional cuts have been done on the cells in order to visualize their adhesion to the substrate. The samples were first fixed with 6% glutaraldehyde in PBS and then gradually dehydrated in ethanol series, immersing them in hexamethyldisilazane (HMDS) as a final step. The cells were gradually cut inside a Zeiss Crossbeam 340 FIB-SEM (focused ion beam-scanning electron microscope) with a Capella Ga FIB, with every slice having a thickness of around 100 nm.

The FIB milling of each slice was performed at a current of 100 pA and a voltage of 30 kV. A dwell time of 200 μs per 3.5 nm^2 pixel was chosen to ensure the milling at the entire depth of one cell and the subjacent fibers. The drift of the ion beam was manually monitored after each slice and corrected, if necessary. An SEM picture of the cross section, in a 54° angle to the Ga-beam, was taken directly after milling each slice to create the image stack.

2.8. Immunostaining and Imaging. Samples were fixed with 4% paraformaldehyde (PFA), permeabilized with 0.05% PBS/Triton-X (PBS-X), and blocked with 1% BSA in PBS. After overnight incubation at 4 °C with the primary antibody directed against vinculin (rabbit, ab73412, Abcam), a Cy3-conjugated goat anti-rabbit secondary antibody (111-165-003, Jackson Immuno-Research) was used for labeling. Nuclei were counterstained with DAPI (Invitrogen), and F-actin was visualized with AlexaFluor 488-conjugated Phalloidin (Thermo Fisher Scientific). Immunofluorescence was analyzed using a Leica TCS SP8 confocal microscope. Images from randomly selected areas of the samples were captured. Fluorescence image processing was performed using FIJI-ImageJ software (NIH).

2.9. Cell Migration. For cell migration experiments, L929 mouse fibroblasts were plated at a density of 30,000 cell/cm^2 on both planar and fibrous PLGA substrates under standard culture conditions. Twenty-four hours after cell seeding, motility was monitored over a period of 6 h using a CytoMate cell analysis system (Cytomate Technologies BV, Netherlands). Cell tracking and quantification were performed using the manual tracking tool in FIJI open software (NIH), and $X–Y$ coordinates were subsequently calculated with Microsoft Excel. Motility maps were obtained by plotting the $X–Y$ coordinates in GraphPad PRISM.

2.10. Surface Wettability. For surface wettability studies, planar glass substrates, PLGA films, and NCO-sP(EO-*stat*-PO)-H-CGRGDS-OH coatings were prepared as described for cell culture experiments and placed at a contact angle measuring device OCA 20 (DataPhysics Instruments GmbH, Germany). A water droplet was dispensed onto the surface of each substrate, and images were taken 5 s after the droplet make contact with the surface. The contact angle was then calculated based on the taken images by use of its corresponding SCA20 software.

3. RESULTS AND DISCUSSION

3.1. Quantification of Immobilized Peptides. On flat surfaces and model substrates, several studies have been performed to quantify cell ligand densities on material surfaces. From these studies, it is well known that the surface density of cell adhesion ligands plays an important role in cell adhesion.[5] We have also previously shown the effects of peptide density on the cell adhesion behavior for hydrogel layers on glass substrates and the challenges for quantification of ligand density at the surface of hydrogels, for example, of sP(EO-*stat*-PO) films.[31] Assays for the surface-sensitive quantification of cell adhesion ligands on fibrous scaffolds, however, are analytically even more challenging. Yet, this information is important if a comparison between 2D and 3D structures that both bear cell adhesion ligands is envisioned. We apply in this work a quantitative, surface-sensitive assay to measure peptide sequences on the surface of the electrospun fibrous meshes by UV-metric means that is based on reductive cleavage of mercaptopyridine-disulfide (Figure S2).

Scheme 1. Principle of Peptide Quantification on the Surface of Fibers[a]
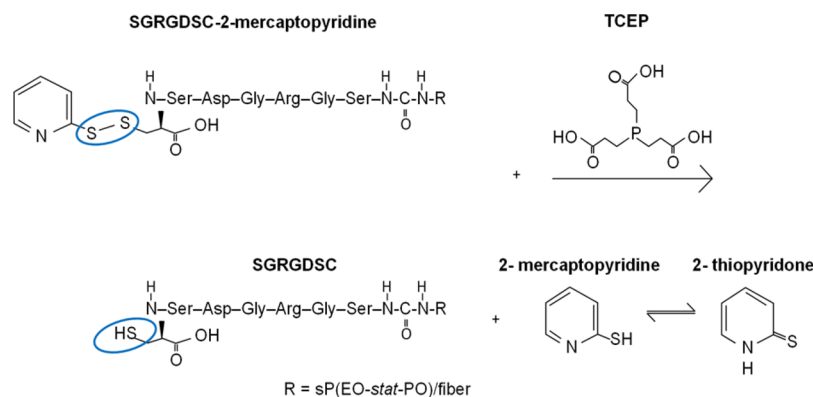
[a]The peptide sequence SGRGDSC with 2-mercaptopyridine at the C-terminus binds to the isocyanate group of NCO-sP(EO-*stat*-PO) on the surface of the fiber. The disulfide bridge within the peptide is cleaved by aqueous TCEP solution. The released amount of 2-mercaptopyridine is equal to the amount of peptide attached to the fiber.

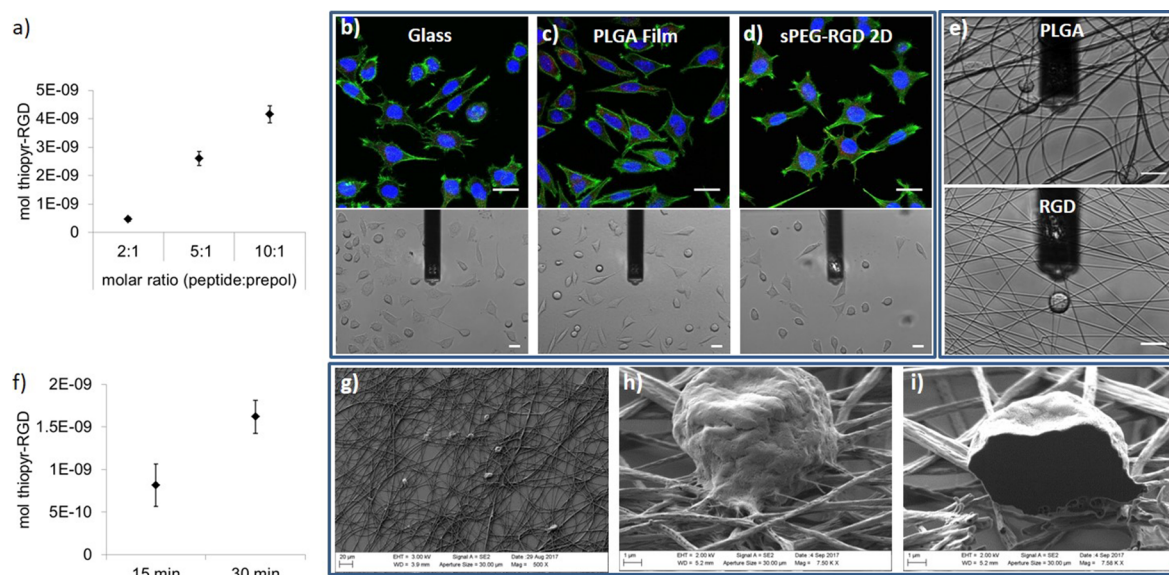**3.2. Quantification of the Amount of Peptide on the Surface of the Fiber.** For straightforward but yet surface-sensitive quantification of peptides, the UV-detectable group 2-mercaptopyridine was linked to the cell binding peptide sequence SGRGDSC via disulfide formation with the thiol group of cysteine. Subsequently, the peptide was used for electrospinning with PLGA and sP(EO-*stat*-PO) (Figure S2a). The peptide can bind covalently to the isocyanate group of sP(EO-*stat*-PO) via the N-terminal serin and is hence present on the surface of the fiber after electrospinning. After spinning, the disulfide bridge between the peptide and 1-mercaptopyridine was cleaved through submerging the mesh in a solution of the reducing agent tris (2-carboxyethyl) phosphine (TCEP) (Scheme 1). Cleaving the disulfide bridge of one peptide yields one free 2-mercaptopyridine, which can rearrange to 2-thiopyridine. Both compounds can be measured in solution quantitatively by UV-spectroscopy showing different UV-absorption maxima at 270 nm (2-mercaptopyridine) and 343 nm (2-pyridothione), respectively.[32] This assay has been recently shown to work with PCL (polycaprolactone) electrospun fibers.[33] Under the conditions used in our study with PLGA-based fibers and under a large excess of TCEP, the intensity ratio between the peaks in a given mixture did not change over time during the quantification procedure. Hence, the amount of SGRGDS bound to the surface of the fibers could be measured by assessment of the 2-mercaptopyridine concentration in solution by UV-spectroscopy through its absorption at 270 nm against a calibration curve. After a first calibration of the absorbance of the mercaptopyridine found in the peptides and that of the pure substance, the correlation between the absorbance and concentration of 2-mercaptopyridine from the peptide was compared with that of pure 2-mercaptopyridine. Both curves were almost identical and showed the same gradient. There was a linear correlation between the solution absorbance and the amount of peptide for concentrations up to at least of 6×10^{-7} mol/mL. Thus, the fiber meshes were immersed in a fixed volume of TCEP solution to reductively break the disulfide bridges in the peptide and release the 2-mercaptopyridine groups, which was calculated by UV-metric analysis of the supernatant. Next, to quantify the amount of peptide located within the fibers, the mesh was degraded by overnight incubation in NaOH; finally, TCEP was added again to release the mercaptopyridine and to measure the amount present in the supernatant (Figure S2b).

Results show that an average of 99% of the peptide is located on the surface of the fibers, while only 1% was embedded in the fibers (Figure 1a).
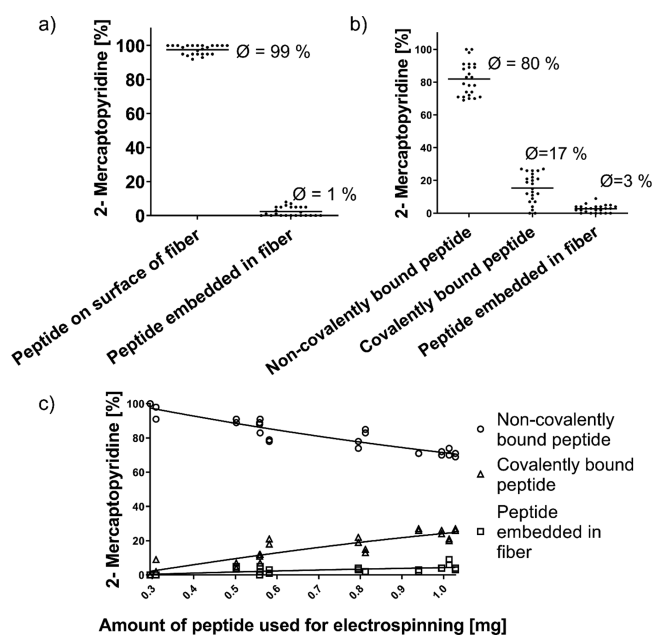
Figure 1. (a) Quantification of the amount of peptide on the surface and within the fibers. (b) Quantification of the peptide amount and binding mode. (c) Influence of the peptide concentration on binding mode.

3.3. Quantification of Peptide Binding Mode. In order to quantify the amount of peptide that is noncovalently attached, covalently bound, and embedded in the fiber, a three-step protocol is followed (Figure S2c). In the first step, the fiber meshes are incubated 24 h in deionized water, the supernatant is then mixed with TCEP and UV-metrically quantified. In this way, the amount of peptide noncovalently attached to the surface of the fiber is calculated. Next, the meshes are incubated in TCEP solution, where the covalently bound groups are released and quantified. Finally, the fibers are incubated in NaOH to be dissolved, and after the addition of TCEP, the amount of peptide embedded in the fibers is quantified UV-metrically. According to our measurements,

Figure 2. (a) Quantification of the amount of peptide on the surface of planar coatings at different peptide to pre-polymer ratios. (b−d upper panels) Spreading of L929 mouse fibroblasts on planar surfaces: glass (b), PLGA film (c), and sP(EO-*stat*-PO)-RGD coating (d), shown by fluorescence images of actin cytoskeleton in green, cell nucleus in blue, and focal adhesions in red (split single channels of the fluorescence images are shown in Figure S6). (b−d lower panels) Bright-field images of living L929 mouse fibroblasts captured during the experiments performed for the quantification of adhesion forces, once the cantilever has approached the cells and right before cell detachment. (e) Bright-field images of living L929 cells seeded on fibrous substrates of PLGA (up) and RGD (down), right before being detached by the cantilever for the measurement of the adhesion force. All scale bars of (b−e) are 25 μm. (f) Quantification of the amount of peptide on the surface of fibers deposited on sP(EO-*stat*-PO) coatings. (g, h) SEM images of L929 cells seeded on fibrous substrates at different magnifications. (i) SEM image of the same cell as in (h), after cutting it with FIB, showing no adherence of the cell to the substrate under the fibers.

Table 1. Projected Area of the Cells on Planar and Fibrous Surfaces and Cell−Substrate Contact Areas

flat substrates			fibrous substrates			
projected cell area = contact area ($\mu m^2 \pm$ s.e.m)			projected cell area ($\mu m^2 \pm$ s.e.m)		contact area ($\mu m^2 \pm$ s.e.m)	
glass	PLGA	sP(EO-*stat*-PO)-RGD	PLGA	sP(EO-*stat*-PO)-RGD	PLGA	sP(EO-*stat*-PO)-RGD
375 ± 10	370 ± 13	382 ± 11	254 ± 11	248 ± 14	50 ± 4	44 ± 2

80% of the total peptide amount is noncovalently bound to the surface of the fibers, 17% of the total peptide is covalently bound to the surface of the fibers, and 3% is embedded in the fiber (Figure 1b).

3.4. Influence of the Peptide Concentration on Binding Mode. In order to evaluate whether the peptide concentration has an influence on the binding mode, resulting in the differences in the amount of peptide embedded within the fibers or immobilized on the surface, the three-step quantification protocol has been performed using different peptide concentrations. Results show that the percentage of peptide embedded inside the fiber does not change substantially upon the increase in the peptide amount. By contrast, on the fiber surface, the noncovalently bound peptide decreases and the covalently bound peptide increases (Figure 1c). This suggests that the reaction between the isocyanate groups and the peptide has not ended during the time that the polymer solution is prepared and electrospun. Moreover, as more peptides are included in the electrospinning solution, the probability to interact with the isocyanate groups is increased and therefore more peptides can covalently attach to NCO-sP(EO-*stat*-PO). At low peptide concentrations, no covalently attached peptide could be determined, which might be due to the minor absorbance of low amounts of peptides. We believe that the peptide concentration was too low to obtain reliable absorption results by UV-spectroscopy.

3.5. Peptide Density and Cell Spreading on Planar Surfaces. Once the material part was set up for the correct characterization of the substrates, we moved on to the biological experiments, with the aim to test the effect of fiber topography on cell adhesion and behavior. First, we started analyzing planar surfaces of different chemistry and wettability, in particular PLGA films, and sP(EO-*stat*-PO) surfaces functionalized with H-CGRGDS-OH, subsequently referred to as sP(EO-*stat*-PO)-RGD, including glass as control. For the quantification of RGD density on the planar surfaces, a two-step version of the above-described protocol has been followed by directly incubating the samples in TCEP solution, without previous washing in water. In this way, every peptide present on the surface is measured at the same time, which includes both the noncovalently and the covalently bound ones. Different molar ratios of peptide/prepolymer have been quantified, more precisely 2:1, 5:1, and 10:1, showing a linear correlation between them (Figure 2a). As a further character-ization, the wettability of the three planar surfaces has been measured using the contact angle of a water droplet, showing the highest wettability on glass and lowest on PLGA surfaces (Figure S3). Having characterized the three planar substrates, they were sterilized and L929 mouse fibroblasts were seeded on them. The spreading of the cells on the substrates was investigated by fluorescence microscopy. As it can be observed, they responded in a very similar way to the three tested
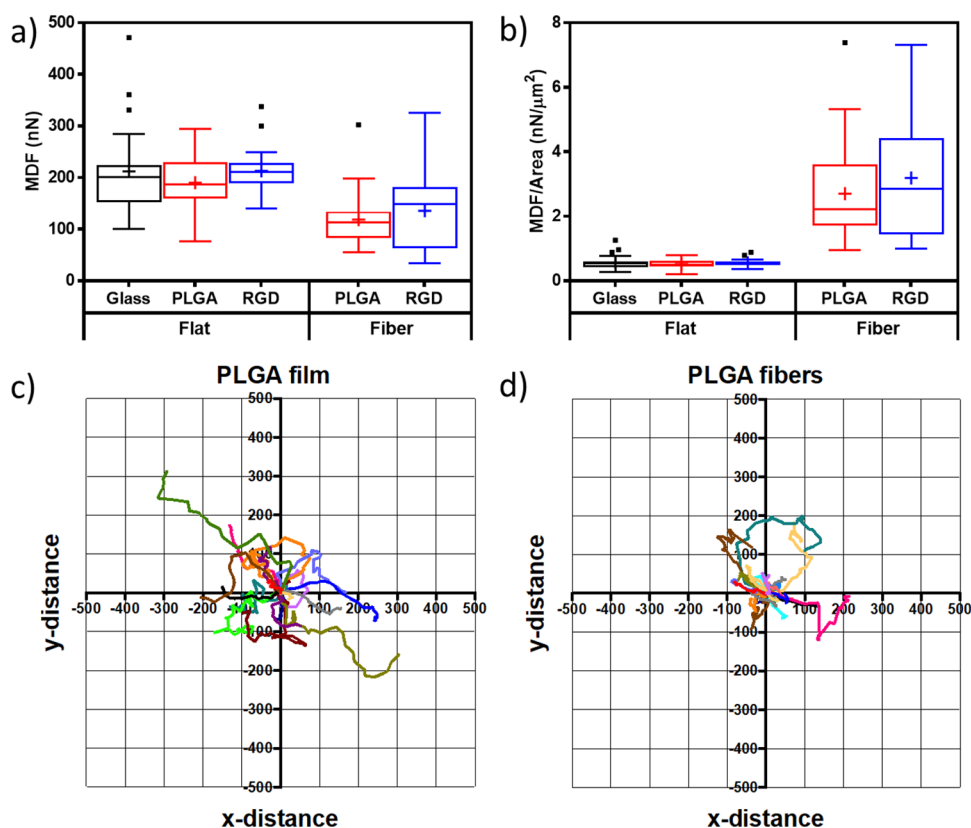
Figure 3. (a) MDF (maximum detachment force) of L929 cells and (b) MDF per area unit, being this area the projected contact area between the cell and the surface. (a) and (b) were measured on planar glass, a PLGA film, and RGD-functionalized sP(EO-*stat*-PO) coatings as well as on fibrous substrates with and without RGD functionalization. In the box-and-whisker plots the center lines indicate medians, the edges of boxes define the 25th and 75th percentiles, "+" indicates mean values, whiskers extend to 1.5 IQR, and dots represent data points below or above the 1.5 IQR. (c) Cell migration on planar PLGA films, 19 cells were tracked in two independent experiments. (d) Cell migration on fibrous PLGA substrates, 22 cells were tracked in four independent experiments.

materials, despite the mentioned differences on surface chemistry and wettability, and they showed no substantial differences in spreading, projected area, stress fibers, and focal adhesions (Figure 2b−d). Moreover, based on the microscopy images, we measured the projected area of the cells, also showing no substantial differences in average values between the three different planar substrates (Table 1).

3.6. Peptide Density and Cell Spreading on Fibrous Surfaces. Transferring the chemical composition of the planar surfaces onto fibrous structures, we electrospun both pristine PLGA and PLGA functionalized with sP(EO-*stat*-PO)-RGD on glass coverslips. In order to avoid cells adhering to the underlying glass, we coated the cover glasses with antifouling sP(EO-*stat*-PO) prior to fiber deposition. In this way, we forced the cells to attach to the fibers alone, thus being able to study the effect of the pure curvature on the cell behavior. The time for electrospinning has been set in such a way that it provides the same fiber density with PLGA fibers as with PLGA-sP(EO-*stat*-PO)-RGD fibers and results in a fiber density low enough to prevent cell infiltration into the fibrous structure (Figure 2e). Due to the low fiber density and the detection limitations of the UV reader, the peptide quantification has been performed on samples that had been electrospun for 30 and 15 min and then the value was extrapolated to the 3 min deposition time used for the biological experiments (Figure 2f). The peptide quantity measured after 30 min of electrospinning provided an average value of 16.2×10^{-10} mol and a value of 8.1×10^{-10} mol after

15 min. Thus, by extrapolation, we conclude that the samples of 3 min deposition time display 1.6×10^{-10} mol of peptide. The projected area of the cells on both fibrous substrates has been calculated and showed very similar values, being slightly smaller the cells cultured on sP(EO-*stat*-PO)-RGD substrates (Table 1). Unlike in previous reports from our group[26] where human fibroblasts seeded on similar substrates widely spread and bridged between fibers, L929 mouse fibroblasts did not assume a spread morphology but instead took a roundish shape on either fibrous material. This distinct behavior in comparison with the human fibroblasts might be due to the cell size and other cellular characteristics such as the ability to stretch and build strong focal adhesions. Many studies concerning fibroblast behavior on various types of substrates containing microscale patterning suggest that cells elongate on such topographical features.[34,35] However, other studies show mouse fibroblasts assuming a spherical shape after seeding onto microtopographical structures.[36] In our study, having the antifouling material underneath the fibers restricts adhesion to the regions where fibers exist.[37] This fact, together with the low fiber density and the characteristics of the cell type used, has led to a roundish shape in the vast majority of the cells grown on the fibrous substrates. Nevertheless, despite the roundish shape, cells proliferated, attached to, and migrated on the fibrous substrates, which indicates that cells are alive and behave normal.

In order to confirm that there is not any cell adhesion to the underlying material, some individual cells grown on the fibrous

substrates were cut into slices using FIB (focused ion beam), while SEM (scanning electron microscopy) images were taken for every slice. This slicing and imaging procedure allowed a three-dimensional reconstruction of the cell, and it revealed that in fact the cells were attached only to the fibers and not to the material underneath (Figure 2g−i and Supplementary Video 1).

3.7. Cell Adhesion Forces and Migration. Once the adhesion of the cells to the fibrous substrates had been assessed, we focused on the differences in cell adhesion forces induced by the topography alone. As a starting point for the biological experiments, in order to facilitate the comparison and interpretation of the results, we decided to ensure the same adhesion force for functionalized and nonfunctionalized equivalents in both planar and fibrous substrates. Therefore, based on previous works of our group and on preliminary setup experiments carried out to establish the experimental conditions (data not shown), the peptide density had been tuned in such a way that it provides a similar cell adhesion force on functionalized surfaces as on its equivalent non-functionalized PLGA surface. Thus, a 2:1 molar ratio (peptide:prepolymer) has been chosen for the planar case and a 1:2 molar ratio for the fibrous case. To estimate the active ligand density values of each surface, we divided the total mole number of conjugated peptides to the active surface area of the respective sample. For the planar sample, the active surface area was taken as the area of 15 mm sP(EO-*stat*-PO)-RGD coated glass coverslips, which yielded a ligand density for the 2:1 peptide:polymer ratio of 2.64×10^{-18} mol/μm^2, which is equal to 15.84×10^{13} ligands/cm^2, which is in good correlation with the values that we reported before that have been obtained with standard quantification techniques.[27] For the fibrous samples, the ligand density was estimated by multiplying the area of the same glass coverslips with fiber density values that were acquired by analyzing SEM images (Figure S4) and an additional correction factor of 1.5 that takes into account the planar projection of the curved fiber surfaces. This resulted in a ligand density of 1.68×10^{-19} mol/μm^2, which is more than 10-fold lower than that for the coated glass slides (Table S1).

The cell adhesion force has been measured by the complete detachment of individual cells from the substrate, achieved as a consequence of the applied constant normal force (Supplementary Video 2 and Figure S7). When comparing the absolute detachment forces, L929 cells presented a very similar adhesion force onto the three planar surfaces (Figure 3a). Likewise, since the projected area of the cells in those surfaces is also very similar (Table 1), it results in the fact that the tension, calculated as the force per contact area, is also very similar in the three planar surfaces (Figure 3b). As occurred before in the study of cell spreading, the differences in chemical composition, wettability, and even rigidity of the studied planar surfaces did not induce major variations in the adhesion force of L929 cells, responding in a very similar way as they do to the glass. These particular results should be highlighted since it has been widely reported that the chemistry, wettability, and energy of the material surface strongly influence cell adhesion.[38] In the planar samples, the projected cell area is at the same time the contact area between the cell and the substrate. On the contrary, in the fibrous case, since the fiber density is very low and the cells attach only to the fibers, the projected area of a cell and the contact area between the cell and the substrate are different. Therefore,

based on microscopy images, we measured both the projected and the contact area, assuming the contact area as the projected area of the segment of the fibers located under the cell (Table 1 and Figure S5). As occurred with the cell projection area, the contact area in sP(EO-*stat*-PO)-RGD-functionalized fibers showed slightly lower values than on PLGA fibers. Nevertheless, a precise calculation of the contact area of each cell selected for detachment is not possible. This limitation leads to inaccuracies in the final values. In terms of detachment forces, the average absolute values presented in both functionalized and nonfunctionalized cases are lower in comparison with the planar cases (Figure 3a). However, when the force per area unit is calculated by introducing the contact area between the cell and the substrate, fibrous substrates present in both cases a significantly higher force density than the planar surfaces (Figure 3b). These results indicate that the topographical cues in this cell type reinforce the cell adhesion strength. A previous work published by Potthoff and co-workers where adhesion forces were measured using the same FluidFM technology as in our work shows also an increase in adhesion force induced by microtopographical structures where human endothelial cells were seeded. Nevertheless, they showed that the cells were spreading out on the structures and there was no antifouling layer underneath. Therefore, the cell adhesion force was influenced by both the geometrical factor as well as by the conformation degree of the cells to the structures or the groove-bridging effect.[17] Our estimation of ligand density on the planar and the fibrous substrates further gives a clear indication that cells can adhere to 3D fibrous substrates already at lower ligand densities, with an overall lower cell−material contact area but still leading to a higher adhesion force density. Even if the ligand density is based on an estimation, this data underlines the strong difference between cell adhesion in 2D and 3D environments. Besides the ligand density of the substrate, Spatz and co-workers have reported the influence of the integrin binding sites on cell adhesion, showing an increase in detachment force with increasing binding site density.[6] A ligand distance of 58 nm favored the recruitment of integrin-associated molecules, leading to integrin lateral clustering, facilitating the formation of focal adhesions and the assembly and colocalization of actin stress fibers.[39]

As the adhesion forces were very similar on PLGA substrates and on sP(EO-*stat*-PO)-RGD substrates, PLGA substrates have been chosen as representative materials to study the influence that these topographical cues might have on cell migration. Migrating cells were recorded for 6 h, taking images every 15 min. Afterward, migration patterns of individual cells were tracked. On the planar surfaces, the migration pattern of some cells was very different compared to other cells; while some of them migrated randomly within small regions, others migrated longer distances with a clearly defined direction. On the fibrous substrates, the migration patterns were more homogeneous, and most of the cells migrated randomly within smaller regions, but all in all, L929 cells migrated longer distances on the planar surfaces than on fibrous ones (Figure 3c,d). These results are in agreement with a previous work published by Shih et al. where a shorter migration distance of MSCs on collagen fibers compared to flat substrates was observed.[40] In our case, unlike in the work of Shih and co-workers where polystyrene culture plates were applied as a flat control, the flat substrate we chose is of the same polymeric material, PLGA, as the fibers. In addition, it has been widely

reported that a well-defined alignment of fibers makes cells migrate faster and longer distances alongside the fiber direction compared to randomly organized fibers or fibers with perpendicular directions, which reduce cell migration.[41−43] Yao and Ding have also reported the influence that the geometrical cues of cell guiding microstripes, such as the width and curvature, have on the migration behavior of the cells.[44] Nevertheless, a direct correlation between migration patterns and adhesion forces cannot be concluded. On the one hand, adhesion forces are mostly related to the integrins engaged in the adhesion and their density, along with adhesion molecules not covered in this study. On the other hand, in this system, migration of the cells is strongly directed by the low density and random distribution of the fibers where they attach, and by the more elongated or rounded shape of the cell itself.

4. CONCLUSIONS

In this study, we have shown that the fibrous topographies reinforce the adhesion strength of cells, while, at low fiber densities, this was not translated into longer migration distances. As the cells were prevented from adhering to the underlying glass and forced instead to attach only to the fibers, the studied fiber distribution led to a reduction in cell spreading. Quantification of the amount of peptide located on the surface of the material as cell adhesion motifs has empowered the comparison between functionalized and nonfunctionalized materials. As key essence of this study, cells can adhere to fibrous substrates with a lower material contact area and at lower cell adhesion ligand density than they need for adhesion on planar substrates and still result in a higher adhesion force per area on the fibrous substrates. In the future, the analysis of cell adhesion-relevant biomarkers via immunochemical staining and further precise localization of such molecules using super-resolution imaging techniques could be a powerful addition. Together, cell adhesion forces and expression and distribution of biomolecules would be a powerful combination to shed light on more intricate cellular processes including differentiation and cancerogenesis.

■ ASSOCIATED CONTENT

ⓢ Supporting Information

The Supporting Information is available free of charge at https://pubs.acs.org/doi/10.1021/acsbiomaterials.1c01290.

> Calibration curve for mercaptopyridine, a scheme of the peptide quantification workflow, wettability measurements of the differently modified planar surfaces, a representative SEM image from the mean fiber density assessment, a scheme of the contact area estimation of cells on the fibers, split channels of the (b−d) upper panels in Figure 2 of the main manuscript, an exemplary curve of the adhesion force exerted by a L929 cell during detachment from a fibrous PLGA substrate, and a table summarizing the active surface area and the ligand density of the substrates (PDF)
>
> Cell slicing by FIB (MP4)
>
> Cell detachment using the FluidFM (MP4)

■ AUTHOR INFORMATION

Corresponding Author

Jürgen Groll − Department of Functional Materials in Medicine and Dentistry at the Institute of Functional Materials and Biofabrication (IFB) and Bavarian Polymer Institute (BPI), University of Würzburg, 97070 Würzburg, Germany; ● orcid.org/0000-0003-3167-8466; Email: juergen.groll@fmz.uni-wuerzburg.de

Authors

Ana Sancho − Department of Functional Materials in Medicine and Dentistry at the Institute of Functional Materials and Biofabrication (IFB) and Bavarian Polymer Institute (BPI), University of Würzburg, 97070 Würzburg, Germany; Department of Automatic Control and Systems Engineering, University of the Basque Country UPV/EHU, 20018 Donostia, Spain

Mehmet Berat Taskin − Department of Functional Materials in Medicine and Dentistry at the Institute of Functional Materials and Biofabrication (IFB) and Bavarian Polymer Institute (BPI), University of Würzburg, 97070 Würzburg, Germany; ● orcid.org/0000-0002-4836-1097

Laura Wistlich − Department of Functional Materials in Medicine and Dentistry at the Institute of Functional Materials and Biofabrication (IFB) and Bavarian Polymer Institute (BPI), University of Würzburg, 97070 Würzburg, Germany

Philipp Stahlhut − Department of Functional Materials in Medicine and Dentistry at the Institute of Functional Materials and Biofabrication (IFB) and Bavarian Polymer Institute (BPI), University of Würzburg, 97070 Würzburg, Germany

Katharina Wittmann − Department of Functional Materials in Medicine and Dentistry at the Institute of Functional Materials and Biofabrication (IFB) and Bavarian Polymer Institute (BPI), University of Würzburg, 97070 Würzburg, Germany

Angela Rossi − Fraunhofer Institute for Silicate Research ISC, Translational Center Regenerative Therapies (TLC-RT), 97070 Würzburg, Germany

Complete contact information is available at:
https://pubs.acs.org/10.1021/acsbiomaterials.1c01290

Notes

The authors declare no competing financial interest.
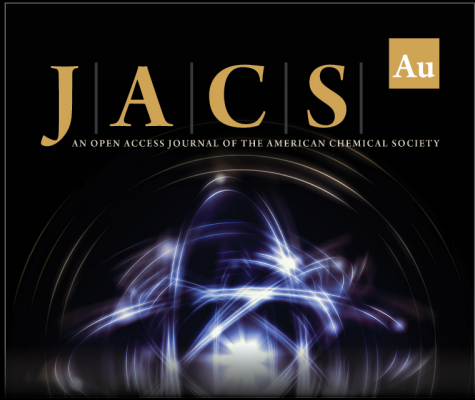
■ ACKNOWLEDGMENTS

■ REFERENCES

(1) Massia, S. P.; Hubbell, J. A. An Rgd Spacing of 440nm Is Sufficient for Integrin Alpha-V-Beta-3-Mediated Fibroblast Spreading and 140nm for Focal Contact and Stress Fiber Formation. J. Cell Biol. 1991, 114, 1089−1100.

(2) Neff, J. A.; Tresco, P. A.; Caldwell, K. D. Surface modification for controlled studies of cell-ligand interactions. Biomaterials 1999, 20, 2377−2393.

(3) Wang, X.; Li, S.; Yan, C.; Liu, P.; Ding, J. Fabrication of RGD micro/nanopattern and corresponding study of stem cell differentiation. Nano Lett. 2015, 15, 1457−1467.

(4) Liu, Q.; Zheng, S.; Ye, K.; He, J.; Shen, Y.; Cui, S.; Huang, J.; Gu, Y.; Ding, J. Cell migration regulated by RGD nanospacing and enhanced under moderate cell adhesion on biomaterials. Biomaterials 2020, 263, 120327.

(5) Deeg, J. A.; Louban, I.; Aydin, D.; Selhuber-Unkel, C.; Kessler, H.; Spatz, J. P. Impact of local versus global ligand density on cellular adhesion. *Nano Lett.* **2011**, *11*, 1469−1476.

(6) Selhuber-Unkel, C.; Erdmann, T.; Lopez-Garcia, M.; Kessler, H.; Schwarz, U. S.; Spatz, J. P. Cell Adhesion Strength Is Controlled by Intermolecular Spacing of Adhesion Receptors. *Biophys. J.* **2010**, *98*, 543−551.

(7) Dalby, M. J.; Gadegaard, N.; Oreffo, R. O. C. Harnessing nanotopography and integrin-matrix interactions to influence stem cell fate. *Nat. Mater.* **2014**, *13*, 558−569.

(8) Gonzalez-Cruz, R. D.; Fonseca, V. C.; Darling, E. M. Cellular mechanical properties reflect the differentiation potential of adipose-derived mesenchymal stem cells. *Proc. Natl. Acad. Sci. U. S. A.* **2012**, *109*, E1523−E1529.

(9) Lulevich, V.; Zink, T.; Chen, H. Y.; Liu, F. T.; Liu, G. Y. Cell mechanics using atomic force microscopy-based single-cell compression. *Langmuir* **2006**, *22*, 8151−8155.

(10) Friedrichs, J.; Helenius, J.; Muller, D. J. Quantifying cellular adhesion to extracellular matrix components by single-cell force spectroscopy. *Nat. Protoc.* **2010**, *5*, 1353−1361.

(11) Weder, G.; Guillaume-Gentil, O.; Matthey, N.; Montagne, F.; Heinzelmann, H.; Voros, J.; Liley, M. The quantification of single cell adhesion on functionalized surfaces for cell sheet engineering. *Biomaterials* **2010**, *31*, 6436−6443.

(12) Taubenberger, A. V.; Hutmacher, D. W.; Muller, D. J. Single-Cell Force Spectroscopy, an Emerging Tool to Quantify Cell Adhesion to Biomaterials. *Tissue Eng Part B-Re* **2014**, *20*, 40−55.

(13) Sankaran, S.; Jaatinen, L.; Brinkmann, J.; Zambelli, T.; Voros, J.; Jonkheijm, P. Cell Adhesion on Dynamic Supramolecular Surfaces Probed by Fluid Force Microscopy-Based Single-Cell Force Spectroscopy. *ACS Nano* **2017**, *11*, 3867−3874.

(14) Potthoff, E.; Guillaume-Gentil, O.; Ossola, D.; Polesel-Maris, J.; LeibundGut-Landmann, S.; Zambelli, T.; Vorholt, J. A. Rapid and Serial Quantification of Adhesion Forces of Yeast and Mammalian Cells. *PLoS One* **2012**, *7*, e52712.

(15) Sancho, A.; Vandersmissen, I.; Craps, S.; Luttun, A.; Groll, J. A new strategy to measure intercellular adhesion forces in mature cell-cell contacts. *Sci. Rep.* **2017**, *7*, 46152.

(16) Guillaume-Gentil, O.; Potthoff, E.; Ossola, D.; Franz, C. M.; Zambelli, T.; Vorholt, J. A. Force-controlled manipulation of single cells: from AFM to FluidFM. *Trends Biotechnol.* **2014**, *32*, 381−388.

(17) Potthoff, E.; Franco, D.; D'Alessandro, V.; Starck, C.; Falk, V.; Zambelli, T.; Vorholt, J. A.; Poulikakos, D.; Ferrari, A. Toward a Rational Design of Surface Textures Promoting Endothelialization. *Nano Lett.* **2014**, *14*, 1069−1079.

(18) Wysotzki, P.; Sancho, A.; Gimsa, J.; Groll, J. A comparative analysis of detachment forces and energies in initial and mature cell-material interaction. *Colloids Surf., B* **2020**, *190*, 110894.

(19) Geiger, B.; Bershadsky, A.; Pankov, R.; Yamada, K. M. Transmembrane crosstalk between the extracellular matrix–cytoskeleton crosstalk. *Nat. Rev. Mol. Cell Biol.* **2001**, *2*, 793−805.

(20) Cukierman, E.; Pankov, R.; Stevens, D. R.; Yamada, K. M. Taking cell-matrix adhesions to the third dimension. *Science* **2001**, *294*, 1708−1712.

(21) Griffith, L. G.; Swartz, M. A. Capturing complex 3D tissue physiology in vitro. *Nat. Rev. Mol. Cell Biol.* **2006**, *7*, 211−224.

(22) Stevens, M. M.; George, J. H. Exploring and engineering the cell surface interface. *Science* **2005**, *310*, 1135−1138.

(23) Groll, J.; Fiedler, J.; Engelhard, E.; Ameringer, T.; Tugulu, S.; Klok, H. A.; Brenner, R. E.; Moeller, M. A novel star PEG-derived surface coating for specific cell adhesion. *J. Biomed. Mater. Res. A* **2005**, *74A*, 607−617.

(24) Groll, J.; Ademovic, Z.; Ameringer, T.; Klee, D.; Moeller, M. Comparison of coatings from reactive star shaped PEG-stat-PPG prepolymers and grafted linear PEG for biological and medical applications. *Biomacromolecules* **2005**, *6*, 956−962.

(25) Ding, J.; Zhang, J.; Li, J.; Li, D.; Xiao, C.; Xiao, H.; Yang, H.; Zhuang, X.; Chen, X. Electrospun polymer biomaterials. *Prog. Polym. Sci.* **2019**, *90*, 1−34.

(26) Grafahrend, D.; Heffels, K. H.; Beer, M. V.; Gasteier, P.; Moller, M.; Boehm, G.; Dalton, P. D.; Groll, J. Degradable polyester scaffolds with controlled surface chemistry combining minimal protein adsorption with specific bioactivation. *Nat. Mater.* **2011**, *10*, 67−73.

(27) Rossi, A.; Wistlich, L.; Heffels, K. H.; Walles, H.; Groll, J. Isotropic Versus Bipolar Functionalized Biomimetic Artificial Basement Membranes and Their Evaluation in Long-Term Human Cell Co-Culture. *Adv. Healthcare Mater.* **2016**, *5*, 1939−1948.

(28) Wistlich, L.; Kums, J.; Rossi, A.; Heffels, K.-H.; Wajant, H.; Groll, J. Multimodal Bioactivation of Hydrophilic Electrospun Nanofibers Enables Simultaneous Tuning of Cell Adhesivity and Immunomodulatory Effects. *Adv. Funct. Mater.* **2017**, *27*, 1702903.

(29) Taskin, M. B.; Ahmad, T.; Wistlich, L.; Meinel, L.; Schmitz, M.; Rossi, A.; Groll, J. Bioactive Electrospun Fibers: Fabrication Strategies and a Critical Review of Surface-Sensitive Characterization and Quantification. *Chem. Rev.* **2021**, 11194.

(30) Groll, J.; Ameringer, T.; Spatz, J. P.; Moeller, M. Ultrathin coatings from isocyanate-terminated star PEG prepolymers: Layer formation and characterization. *Langmuir* **2005**, *21*, 1991−1999.

(31) Beer, M. V.; Hahn, K.; Diederichs, S.; Fabry, M.; Singh, S.; Spencer, S. J.; Salber, J.; Moller, M.; Shard, A. G.; Groll, J. Quantifying ligand-cell interactions and determination of the surface concentrations of ligands on hydrogel films: The measurement challenge. *Biointerphases* **2015**, *10*, 021007.

(32) Grassetti, D. R.; Murray, J. F. Determination of Sulfhydryl Groups with 2,2'- or 4,4'-Dithiodipyridine. *Arch. Biochem. Biophys.* **1967**, *119*, 41−49.

(33) Blum, C.; Taskin, M. B.; Shan, J.; Schilling, T.; Schlegelmilch, K.; Teßmar, J.; Groll, J. Appreciating the First Line of the Human Innate Immune Defense: A Strategy to Model and Alleviate the Neutrophil Elastase-Mediated Attack toward Bioactivated Biomaterials. *Small* **2021**, 2007551.

(34) Charest, J. L.; Garcia, A. J.; King, W. P. Myoblast alignment and differentiation on cell culture substrates with microscale topography and model chemistries. *Biomaterials* **2007**, *28*, 2202−2210.

(35) Nikkhah, M.; Edalat, F.; Manoucheri, S.; Khademhosseini, A. Engineering microscale topographies to control the cell-substrate interface. *Biomaterials* **2012**, *33*, 5230−5246.

(36) Weder, G.; Blondiaux, N.; Giazzon, M.; Matthey, N.; Klein, M.; Pugin, R.; Heinzelmann, H.; Liley, M. Use of Force Spectroscopy to Investigate the Adhesion of Living Adherent Cells. *Langmuir* **2010**, *26*, 8180−8186.

(37) Yao, X.; Peng, R.; Ding, J. Cell-Material Interactions Revealed Via Material Techniques of Surface Patterning. *Adv. Mater.* **2013**, *25*, 5257−5286.

(38) Bacakova, L.; Filova, E.; Parizek, M.; Ruml, T.; Svorcik, V. Modulation of cell adhesion, proliferation and differentiation on materials designed for body implants. *Biotechnol. Adv.* **2011**, *29*, 739−767.

(39) Cavalcanti-Adam, E. A.; Micoulet, A.; Blummel, J.; Auernheimer, J.; Kessler, H.; Spatz, J. P. Lateral spacing of integrin ligands influences cell spreading and focal adhesion assembly. *Eur. J. Cell Biol.* **2006**, *85*, 219−224.

(40) Shih, Y. R. V.; Chen, C. N.; Tsai, S. W.; Wang, Y. J.; Lee, O. K. Growth of mesenchymal stem cells on electrospun type I collagen nanofibers. *Stem Cells* **2006**, *24*, 2391−2397.

(41) Johnson, J.; Nowicki, M. O.; Lee, C. H.; Chiocca, E. A.; Viapiano, M. S.; Lawler, S. E.; Lannutti, J. J. Quantitative Analysis of Complex Glioma Cell Migration on Electrospun Polycaprolactone Using Time-Lapse Microscopy. *Tissue Eng Part C-Me* **2009**, *15*, 531−540.

(42) Mi, H. Y.; Salick, M. R.; Jing, X.; Crone, W. C.; Peng, X. F.; Turng, L. S. Electrospinning of unidirectionally and orthogonally aligned thermoplastic polyurethane nanofibers: Fiber orientation and cell migration. *Journal of Biomedical Materials Research Part A* **2015**, *103*, 593−603.

(43) Nelson, M. T.; Short, A.; Cole, S. L.; Gross, A. C.; Winter, J.; Eubank, T. D.; Lannutti, J. J. Preferential, enhanced breast cancer cell

migration on biomimetic electrospun nanofiber 'cell highways'. *BMC Cancer* **2014**, *14*, 1−16.

(44) Yao, X.; Ding, J. Effects of Microstripe Geometry on Guided Cell Migration. *ACS Appl. Mater. Interfaces* **2020**, *12*, 27971−27983.